Organic Photosensor in Elgraphy (I): Amplification of Photocurrent and its Mechanism

D. Aoki,▲ M. Okabe, S. Hikosaka, and E. Inoue▲

Central Research Institute Dainippon Printing Co., Ltd., Chiba-Ken, Japan

The authors are actively involved in the development of Elgraphy: a novel image acquiring system that combines electrophotography and liquid crystal technology. The intermediate medium for image storage in Elgraphy (image receptor) consists of an organic photosensor layer (Elgraphic photosensor) and a liquid-crystal layer. The Elgraphic photosensor, through which a dark current of several $\mu A/cm^2$ flows when a voltage of 10 V/μm is applied at room temperature, exhibits marked photocurrent amplification: exposure to light yields a photocurrent greater than the number of photons absorbed. Upon exposure to light, the quantum yield rises very fast and exceeds unity within about 30 msec. The ionization potential of the charge transfer material (CTM) are shown to be related to photocurrent amplification. The state of space charges trapped in the photoconductive layer is probably affected by the diffusion of the CTM into the charge generation layer (CGL). It has been found that several types of deep traps with a trap depth of more than 1 eV play an important role in this phenomenon. The authors propose that these traps capture electrons generated near the electrode/photoconductive layer interface, thus lowering the barrier to hole injection.

Introduction

Elgraphy is a novel high resolution, high sensitivity image acquiring system utilizing dry processes. The image receptor in the system consists of a photosensor (Elgraphic photosensor), an intermediate layer, and a memory-type liquid-crystal layers[1–3] (Fig. 1). The Elgraphic photosensor exhibits photocurrent amplification characteristics,[4] that is, the ratio of the number of incident photons to the number of electrons, which was estimated from the magnitude of the photoinduced current exceeds the number of input photons.

Nakatani, Hanna, Kokado, and co-workers[5,6] reported the effect that negative space charges that accumulate in the charge generation layer have on electrophotographic characteristics, such as the charge acceptance and the sensitivity, in stacked organic photosensitive materials. The photocurrent amplification observed in Elgraphy may also be ascribed to a similar space charge distribution. This article describes the characteristics of the photocurrent amplification in Elgraphy and attempts to explain the driving mechanism.

Experimental

Fabrication of Photosensor

Figure 2 shows the configuration of the Elgraphic photosensor. Two charge conducting layers, an organic charge generation layer (CGL), followed by a charge carrier transport layer (CTL), are stacked on a transparent electrode formed on a glass substrate. The CGL generates photocarriers and the CTL transports them.

The fabrication steps are as follows. Various types of electrodes (Table I), were deposited on cleaned glass substrates.

After the surface is cleaned, it is coated with a CGL layer by spreading an ink consisting of charge generation material (CGM), bis-azo pigment material (Dainichiseika Color & Chemicals MFG. Co., Ltd., Japan), shown below, dispersed in polyvinylformal resin (3:1 by weight) to a thickness of 0.3 μm, and drying for an hour at 100°C .

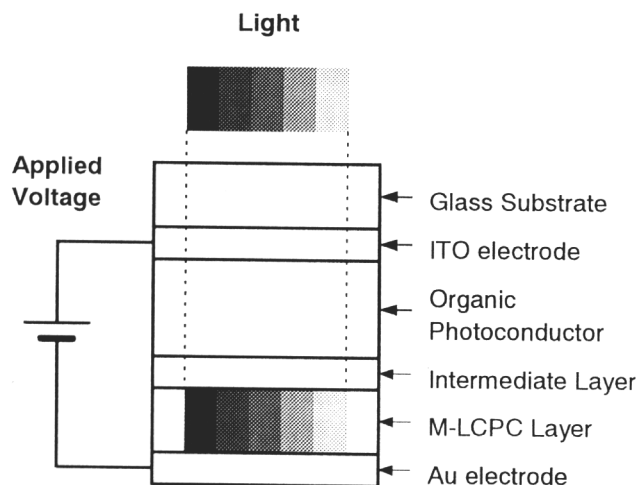A CTL layer is formed on top of the CGL layer. Several types of charge transfer materials (CTM) were

**Figure 1.** Structure and configuration of image receptor.

TABLE I. Various Types of Electrode

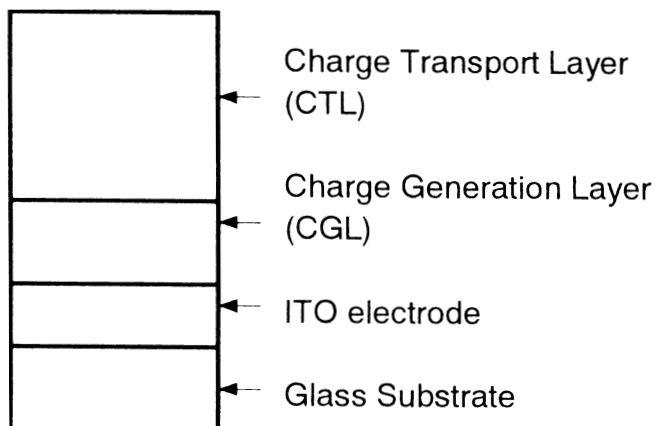| Electrode	Deposition	Resistance (Ω/sq)	Thickness (A)	Transmittance (%)
Indium-tin oxide (ITO)	electron beam evaporation	100	1000	>90;
Tin oxide (SnO$_2$)	electron beam evaporation	100	1000	>90;
Zinc oxide (ZnO)	sputtering	1000	700	70-80
Gold (Au)	evaporation	<10	<100	60
Aluminum (Al)	evaporation	<10	<100	60
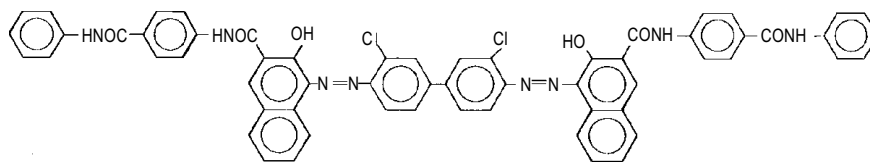
CGM: bis-azo pigment

Figure 2. Structure of photosensor.

mixed with polycarbonate resin (Eupiron Z400: Mitsubishi Gas Chemicals, Japan) in a ratio of 3:1 by weight. The mixtures were dissolved in a solvent mixture consisting of dichrolomethane and 1,1,2-trichloroethane, and were then spin coated on the substrate, and dried for two hours at 80°C in a clean oven. The amount applied was such that the final thickness was 10 μm after drying. Measurements were made after storing the sensor unit for three days in the dark.

Measurement of Photocurrent

A measuring cell was made by evaporating a 4 mm × 4 mm Au electrode on the CTL surface. The circuit shown in the previous article[3] was used to measure the photocurrent and dark current. A constant DC voltage was applied across the cell, and light with a wavelength of 560nm from a monochromator illuminated the cell while the photocurrent was monitored on an oscilloscope. All measurements were made at room temperature.

Calculation of Quantum Yield

The photoinduced current is defined to be the current obtained by subtracting the dark current from the photocurrent. The quantum yield η(t) is defined to be the ratio of the number of incident photons to the number of photogenerated electrons, estimated from the magnitude of the photoinduced current. The incident light had a

wavelength of 560 nm and an intensity of 10 μW/cm^2 (2.82 × 10^{13} photons/cm^{2}sec). The quantum yield is given by:

$$\eta(t) = \frac{6.24 \times 10^{18} \times \int_0^t I(t)dt}{2.82 \times 10^{13} \times t} \qquad (1)$$

where t is the exposure time (sec.), and $I(t)$ is the induced current (A/cm^2).

Measurement of Work Function and Ionization Potential

The work function of the electrode material and the ionization potential of the CGM and CTM were measured with an atmospheric photoelectron emission analyzer[7] (AC-1, Riken Keiki Manufacturing, Japan). The intensity of the illumination ranged from 10 to 1000 mW.

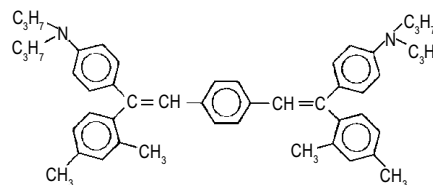**Measurement of Thermally Stimulated Current (TSC)**

The thermally stimulated current (TSC) of a photosensor with a 4 mm × 4 mm Au electrode was measured with short circuit TSC measuring equipment (Souyou Seiki Manufacturing Co., Ltd.). The photosensor was heated at a constant rate while the ITO electrode was grounded and a bias of –2 V was applied.

Results and Discussion

Transient Characteristics of Quantum Yield

A Photosensor was fabricated by forming CGL and CTL layers on top of the ITO electrode. The dibutadienylbenzene derivative (DBB: bis-dimethylphenyldipropylaminophenylbenzene, Takasago International Corporation, Japan) shown below was used as the CTM.
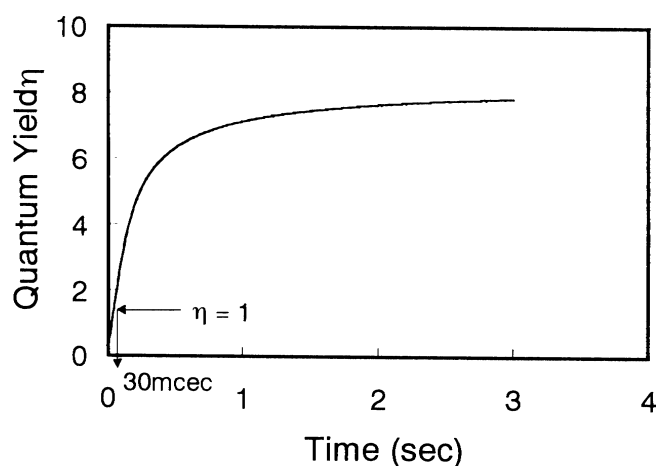

CTM: di-butadienilbenzene derivative (DBB)

A measuring cell was exposed to light (560 nm, 10 μW/cm^2) while a 120 V DC voltage was applied across it. Figure 3 shows how the photocurrent and dark cur-
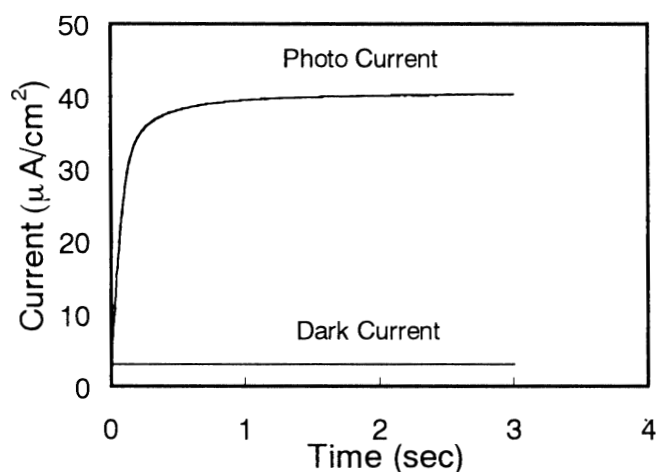
Figure 3. Current-time characteristics of the photo sensor in dark and light. The sensor was exposed by light 560 nm, 10 µW/cm² at 120 V applied.

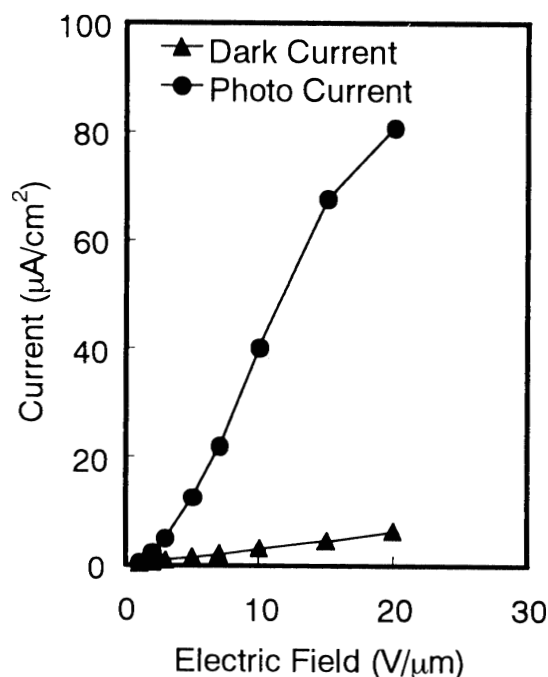**Figure 4.** Change of quantum yield by light exposure (560 nm, 10 µW/cm²) at 120 V applied.

Figure 5. I-V characteristics of photosensor. The exposure condition: 560 nm, 10 µW/cm² for 3 sec.

Figure 6. Quantum yield versus electric field of photosensor. The exposure light was 560 nm, 10 µW/cm².
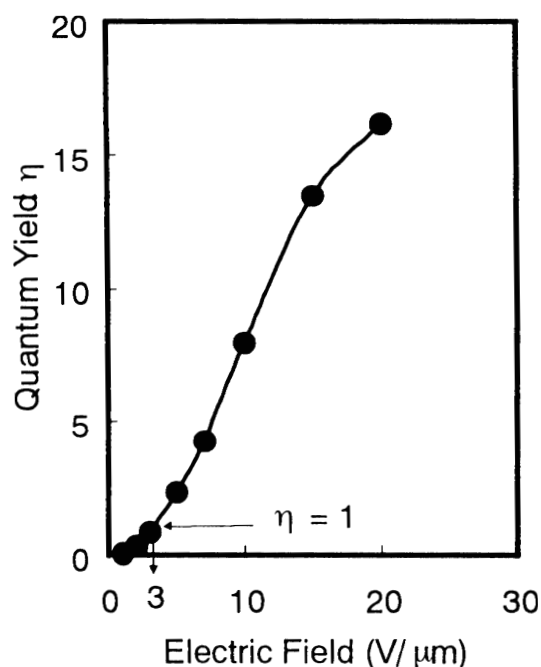
rent change over time. When illumination began, the photocurrent rose sharply and saturated after about one second, while the dark current did not change significantly during the experiment. Figure 4 shows how the quantum yield calculated from the photoinduced current (dark current subtracted from photocurrent) varies over time. It exceeded unity within 30 msec after illumination began, and continued to rise until it reached the saturation value of 8.

Electric Field Dependence of Quantum Yield

A measuring cell was exposed to light (560 nm, 10 µW/cm²) while the voltage applied to the cell (across the photosensor) was changed. Figure 5 shows how the photocurrent and dark current changed in the first three seconds after illumination began. The dark current rose as the applied voltage increased, and current injection from the ITO electrode was observed. The photocurrent increased at a greater rate than the dark current. The quantum yield calculated from the photoinduced current (dark current subtracted from photocurrent) is shown in Fig. 6. It exceeded unity at a field strength of 3 V/µm, and continued to rise as the applied field be-

came stronger. It reached a value of around 17 at 20 V/µm, and then gradually leveled off.

Amplification phenomena due to tunneling have been reported[8] to have a definite threshold voltage, which gives rise to the amplification: the quantum yield rises sharply when a high electronic field of several tens of V/µm is applied. In sharp contrast to that behavior, the Elgraphy photosensor does not exhibit a definite voltage threshold, and amplification was observed at fields as low as several V/µm.
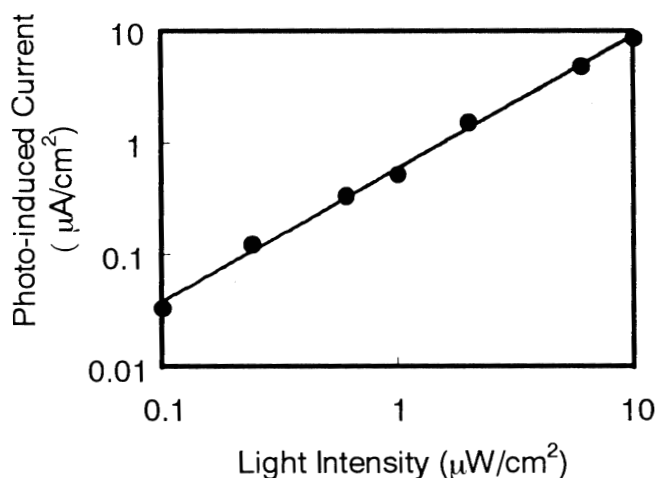
Figure 7. Photo induced current versus light intensity. The exposure time was 33 msec by applying a 120 V DC voltage.

Relationship of Light Intensity and PhotoInduced Current

Figure 7 shows the relationship between the intensity of the illumination and the photoinduced current for 560 nm monochromatic light. The photoinduced current increases linearly with the intensity. In the previous article,[3] we reported that the deposition of SiO_2 eliminated the photocurrent amplification. This fact suggests that, in the Elgraphic photosensor, the level of hole injection from the ITO electrode is proportional both to the illumination intensity and to the number of photocarriers generated in the CGL layer.

Work Function of Electrode Material

Because light illuminates an Elgraphic photosensor from the glass substrate side, the electrode must be transparent. Table II shows the values of the work function (ϕ_M) obtained from the surface analyzer (AC-1) for several types of electrodes formed on glass substrates.

Photosensors were fabricated by forming CGL and CTL layers on top of these electrodes. The hydrazone derivative (HDZ) shown below was used as the CTM, whose ionization potential is 5.21 eV.
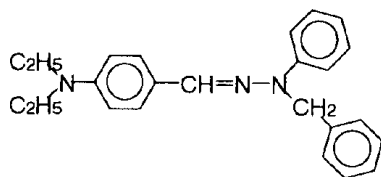

Hydrazone derivative (HDZ)

The dark current and photocurrent of the photosensors were measured while a DC bias of 150 V (equivalent to 15 V/µm) was applied, and the photosensors were illuminated with monochromatic light with a wavelength of 560 nm and an intensity of 3.0 µW/cm² for 33 msec.

In Fig. 8, the magnitudes of the photo and dark currents 33 msec after illumination began are plotted against the work function of the electrodes. Increases in both currents and photocurrent amplification appear when the work function is greater than 4.60 eV.

However, for ZnO, which has a 4.60 eV work function, the photocurrent increased abruptly when the intensity of the illumination was raised to 15 µW/cm² and the ex-

TABLE II. Work Function of Electrode

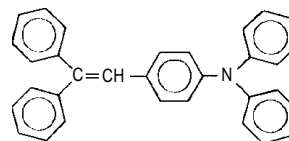| Electrode	ϕ_M (eV)
Al	4.02
ZnO	4.62
ITO	4.75
SnO₂	4.80
Au	4.83
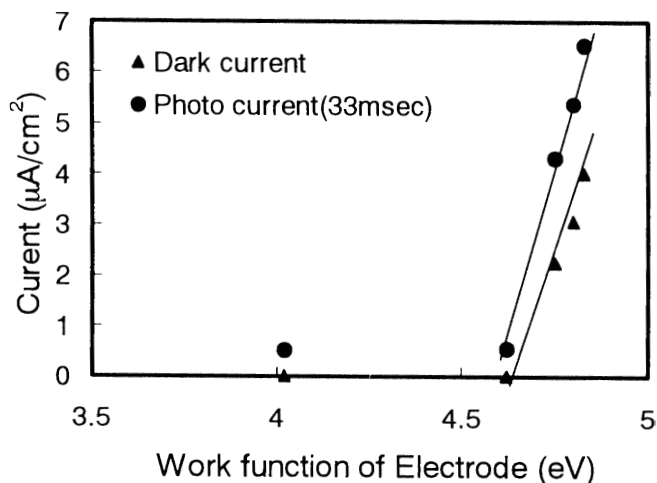
Figure 8. Photo and dark current plotted against the work function of electrode. Applied voltage was 150 V DC. The light exposure at 560 nm, was 3.0 µW/cm² for 33 msec.

posure time was prolonged (Fig. 9). The photocurrent also decayed more slowly as the exposure time became longer. This is probably due to hole injection from the electrode induced by space charges which accumulate to a certain extent as the exposure time becomes longer.

Figure 10 shows a band diagram of the electrode/CGL interface. The CCL valence band is assumed to be the ionization potential of bis-azo pigment, which was calculated from the same kind of measurements. The CGL conduction band was estimated from the absorption edge. The height of the barrier to hole injection is given by $\phi_{CGM} - \phi_M$. As the work function of the electrode increases, $\phi_{CGM} - \phi_M$ becomes smaller, thus inducing hole injection from the electrode.
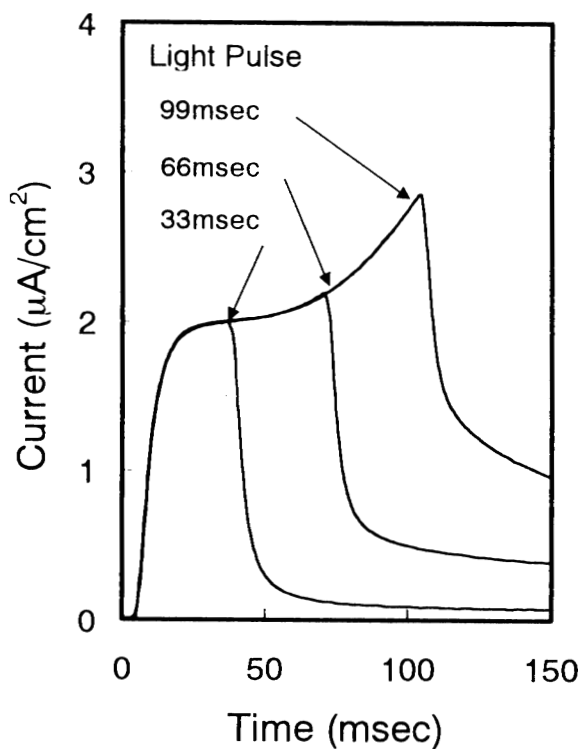
Ionization Potential of CTM

CTMs have various types and numbers of substitutional groups. The basic structures are shown below.

Type-1
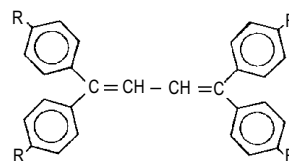
Type-2

Figure 9. Characteristics of photocurrent with light exposure at 560 nm, were 15 $\mu W/cm^2$ for 33 msec, 66 msec, and 99 msec, respectively, when zinc oxide was used in the photosensor electrode. Applied voltage was 150 V DC.
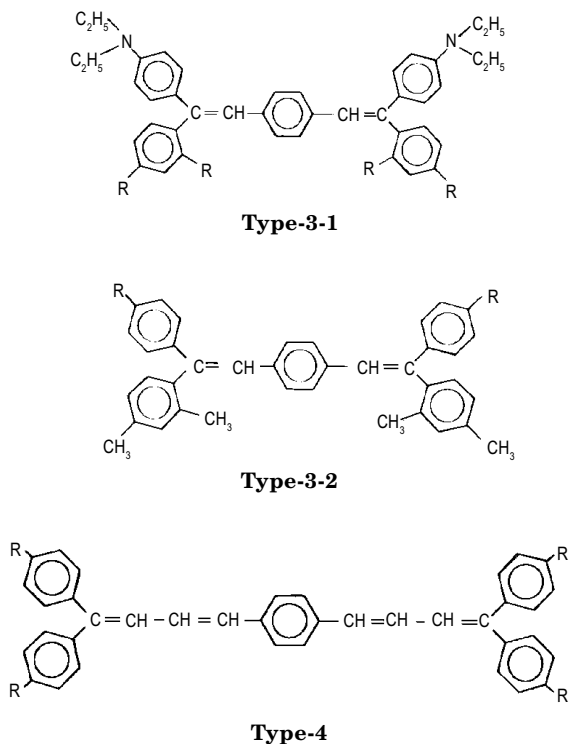

Type-3-1

Type-3-2

Type-4

Table III shows their measured ionization potentials (ϕ_{CTM}). As the π-electron conjugated chain becomes longer, as in a Type-4 compound, ϕ_{CTM} tends to decrease. The addition of an electron donor functional group, such

TABLE III. Ionization Potential of Various CTM

CTM	−R	Number of groups	ϕ_{CTM} (eV)
Type-1		0	5.70
Type-2	−OMe	2	5.86
	−NEt₂,	1	5.41
	−NPh₂	1	
	−NMe₂	2	5.18
	−NEt₂	1	5.54
	−NEt₂	2	5.11
	−NEt₂	3	4.83
	−NPr₂	2	5.07
Type-3-1	−H	4	>6.50
	−OMe	4	6.03
	−CH₃	4	5.10
Type-3-2	−NEt₂	2	6.03
	−NPr₂	2	5.11
	−NBu₂	2	5.09
	−NEt₂,	1	5.15
	−NPr₂	1	
Type-4	−NEt₂	4	5.03
	−NBu₂	4	4.77
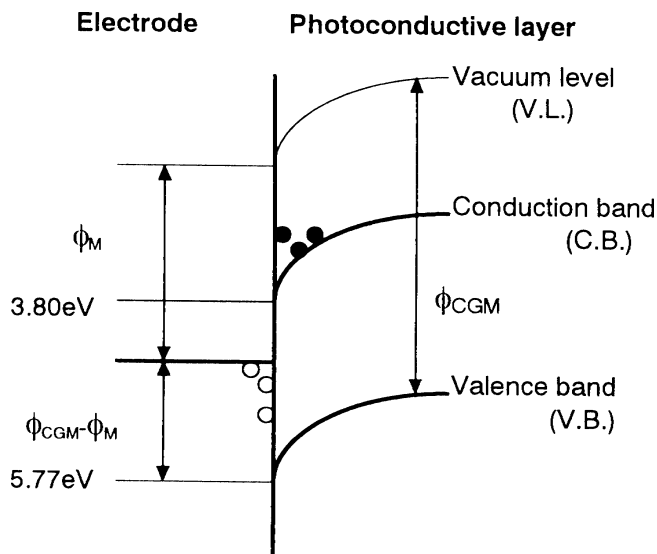
**Figure 10.** Energy band model of the contact state of electrode and photoconductor.
○ hole, ● electron
ϕ_M: Work function of electrode
ϕ_{CGM}: Ionization potential of CGM
$\phi_{CGM} - \phi_M$: Hole injection barrier from electrode to CGL

as OCH_3, CH_3 or an alkylamino group, also tends to reduce ϕ_{CTM}. Type-2 compounds have a relatively small ϕ_{CTM} because they have additive electron donor groups attached. Type-2 and Type-3 compounds also exhibit decreasing ϕ_{CTM} when they have longer alkyl chains in their alkylamino groups.

The effect of ϕ_{CTM} on the electrical characteristics was examined using photosensors with CTL layers, each containing one of several types of CTMs. All the sensors had the same basic layer structure: an ITO electrode and a CGL using bis-azo pigment. The CTL was made by mixing CTM and polycarbonate resin in a ratio of 5:1 by weight. Figure 11 shows a graph of the photo and dark currents versus ϕ_{CTM}. The values of the photocurrent were obtained under monochromatic illumination
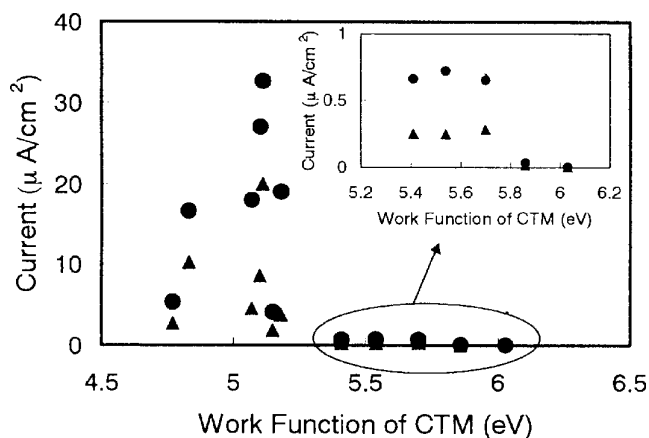
Figure 11. Dark and photo current plotted against the work function of the CTM. The light exposure at 560 nm, was 3.0 μW/cm² for 33 msec. Applied voltage was 150 V DC. ▲ Dark current, ● Photo current

Figure 12. Dark current change by aging in air and nitrogen atmospheres. Applied voltage was 150 V DC.

(560 nm, 3.0 μW/cm²) for 33 msec and an applied DC bias of 150 V.

In the region where ϕ_{CTM} is greater than ϕ_{CGM} (5.77 eV), no photocurrent was observed because hole injection from the CGL to the CTL was suppressed. In the region where ϕ_{CTM} falls between 5.40 and 5.70 eV, a photocurrent was observed, but blocking characteristics also appeared. In the region where ϕ_{CTM} is less than 5.40 eV, the photo and dark currents increased while ϕ_{CTM} became smaller, indicating photocurrent amplification. These results suggest a close relationship between ϕ_{CTM} and hole injection from the electrode, indicating that it might be possibile to obtain any desired photosensor characteristics by choosing an appropriate CTM.

Effect of Oxygen
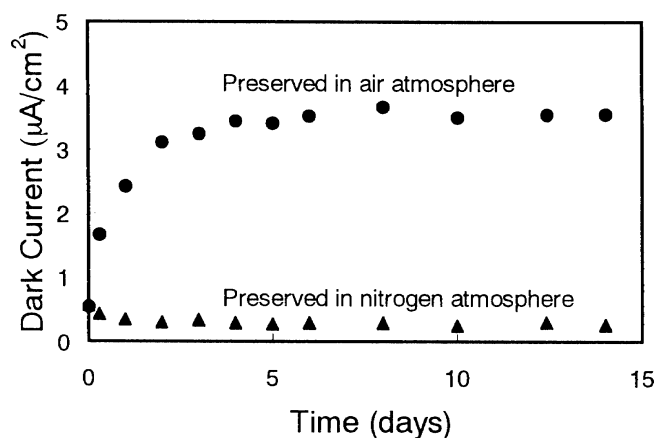### Change in Dark Current over Time

Figure 12 shows how the dark current changed over time for these sensors. In Elgraphic photosensors with a CTM containing DBB (small ϕ_{CTM}), although the sensors initially exhibited blocking characteristics immediately after fabrication, the dark current gradually increased and photocurrent amplification appeared after the sensors were allowed to stand for several day in the atmosphere at room temperature.

The same types of photosensors were stored after fabrication in a nitrogen atmosphere at room temperature. When the sensor was stored after fabrication in a nitrogen atmosphere the dark current did not increase, nor was photocurrent amplification observed.

The dark current of sensors that had been stored in air tended to decrease when placed in a nitrogen atmosphere, while no such tendency was observed for their counterparts placed in a dry atmosphere (H_2O vapor pressure < 1 ppm). This strongly indicates that oxygen affects the behavior of the injection barrier at the electrode/photoconductive layer interface.

Interaction between Oxygen and Charge Transfer Material

Oxygen adsorption at the electrode/CGL interface has been reported to affect the generation of photocarriers in OPCs with a CGM containing phthalocyanine pigment.[9] In the Elgraphic photosensor, the following re-

actions are thought to take place between a CTM with a small ϕ_{CTM} and oxygen molecules:

$$CTM \rightarrow CTM^* + e \qquad O_x + e \rightarrow O_x^- \qquad (2)$$

For a CTM with a small ϕ_{CTM}, oxygen molecules in the air (which can act as acceptors for the CTM that diffused into the CGL) gradually penetrate the electrode/photoconductor interface and are absorbed in accordance with the reactions described above. They are thought to be the cause of the gradual increase in the dark current of photosensors stored in air. The system is thought to attain equilibrium in a few days.

### Addition of Electron Acceptor to the Photosensor with Light Ionization Potential CTM

A combination of bis-azo pigment and a CTM with an ionization potential (ϕ_{CMT}) higher than 5.40 eV was shown to have blocking characteristics. In this experiment, electron acceptor material (2,3-dichloro-5,6-dicyano-p-benzoquinone, DDQ) was added to the CGL (0.5 mol DDQ to 1 mole CGM) of a photosensor with a stilbene derivative CTM (STL, $\phi_{CMT} = 5.70$ eV).

Figure 13 shows the photocurrent response of the photosensor with DDQ and the photosensor without DDQ to pulsed illumination. In this figure, the addition of the electron acceptor was found to increase the darkcurrent and enhance photocurrent amplification. This fact indicates that photocurrent amplification can be controlled by the addition of electron acceptors to the CGL, with the mechanism involved being electron trapping inside the CGL.
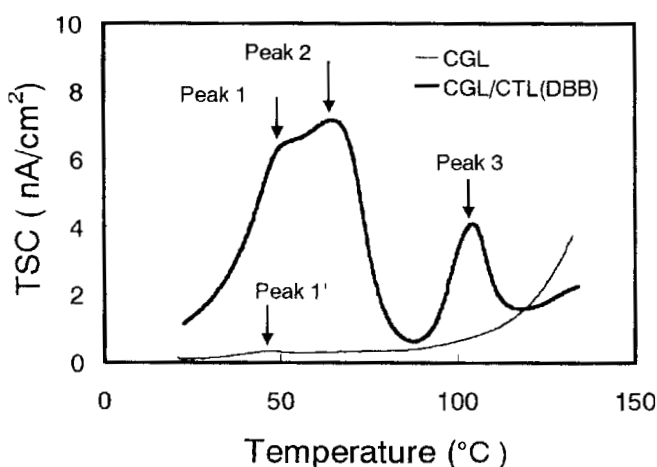
Discussion of Photocurrent Amplification Mechanism
TSC Response of Amplifiying Photosensor

Two layers were formed on the ITO electrode using bis-azo pigment for the CGM and DBB for the CTM. For comparison, the same measurements were made using a monolayer photosensor with just a CGL on the ITO electrode. Figure 14 shows a TSC profile for a heating rate of 5°C/min. Three TSC peaks were observed for the laminated sensor: Peak 1 at 50°C, Peak 2 at 65°C, and Peak 3 at 104°C. In contrast, only a single peak was observed for the monolayer sensor: Peak 1′
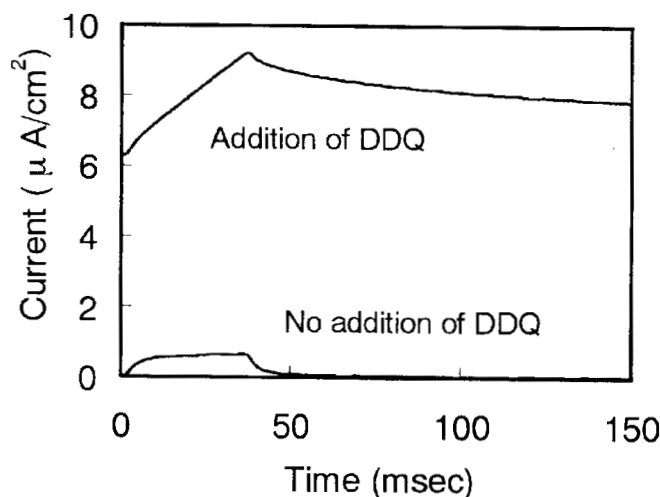
Figure 13. Photocurrent response of the photosensor with acceptor DDQ. Applied voltage was 150 V DC. The light exposure at 560 nm, was 3.0 μW/cm² for 33 msec.

Figure 15. $1000/T_m$ versus $-\ln(\beta/T_m^2)$ plot from the data of Fig. 14

Figure 14. TSC curves of CGL and CGL/CTL.

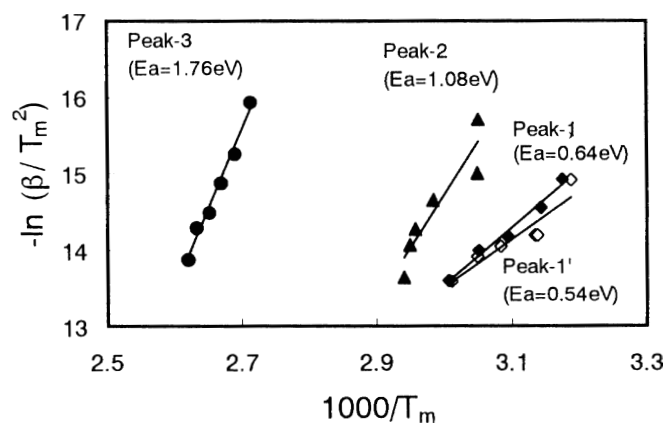**Figure 16.** Energy diagram of Elgraphy photosensor.

at 46°C. When measurements are made just after the laminated sensor is heated to 120°C, no TSC peaks appear; and no photocurrent amplification is observed, either.

These data can be explained as follows: The space charges that have accumulated in the photosensor are flushed and the photosensor returns to its initial state, as just after fabrication. After the sensor is allowed to stand for several days, TSC peaks appear and photocurrent amplification is also observed. This reveals a close relationship between photocurrent amplification and the TSC peaks, and the amplification mechanism is probably related to space charges that accumulate in the photoconductive layer over time.
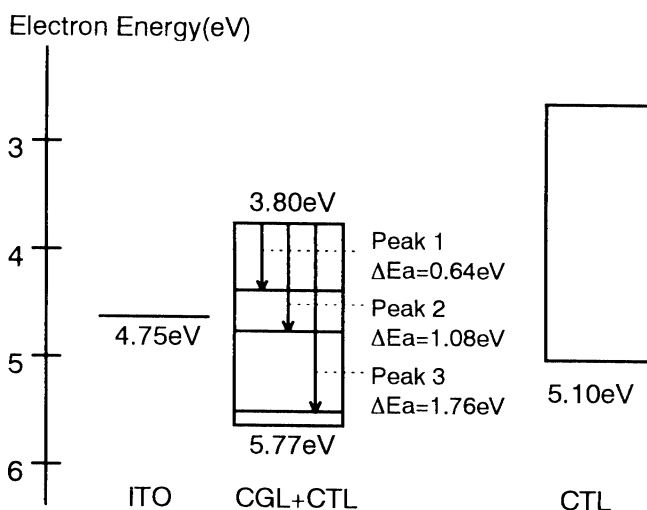
Activation Energy of Traps from TSC Measurements

The following equation relates TSC measurement parameters:[10]

$$\ln\frac{\beta}{T_m^2} = \ln\frac{k}{E_a\tau_0} - \frac{E_a}{kT_m} \qquad (3)$$

where T_m is the absolute temperature at which a TSC peak occurs, β is the heating rate, E_a is the activation energy of traps, k is Boltzmann's constant, and τ_0 is the inverse of the electron frequency. Measurements were made at various heating rates ranging from 2 to 10°C/min, and $\ln(\beta/T_m^2)$ was plotted against $1/T_m$. The curves are linear (Fig. 15), and the activation energy of traps was estimated from the slopes of the lines.

Peak 1 of the laminated sensor and Peak 1′ of the monolayer sensor exhibited similar behavior, as shown in Fig. 15, suggesting that they are produced by the same trap in the CGL. Peaks 2 and 3 result from the mixing of the CTM into the CTL (or from the formation of a thin CTM layer), and the estimated activation energies (1.08 and 1.76 eV) indicated that they composed to deep traps.

Figure 16 is an energy diagram for a laminated photosensor. In light of the activation energy (ΔE_a) for Peak 2 (1 eV), this peak is assigned to traps created by absorbed oxygen, as described above. The activation energy for Peak 3 is just above the valence band and has a strong electron receptor capability. This trap typi-

Aoki, et al.
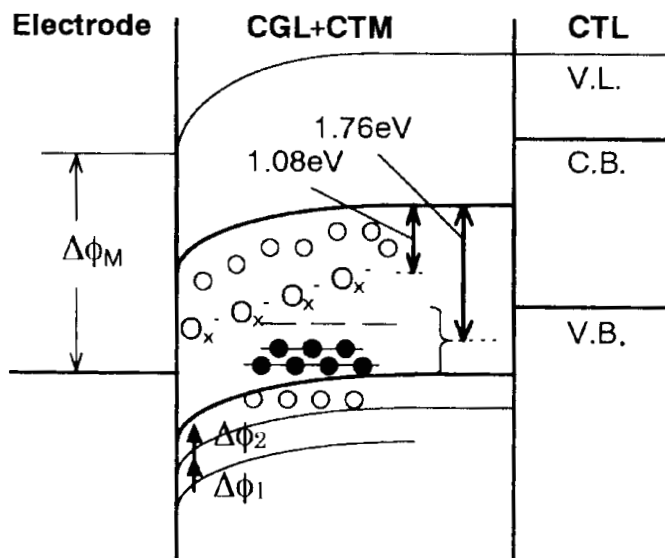
Figure 17(a). Band diagram of Elgraphic photosensor after aging in air without light exposure or applied voltage. Thermal carriers are trapped at oxygen and other deep traps. ○ hole, ● electron
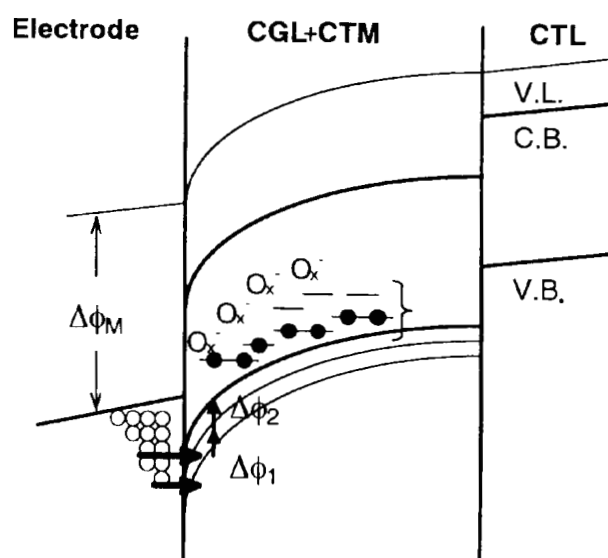
Figure 17(b). Hole injection from electrode to photoconductive layer with applied voltage only. ○ hole, ● electron
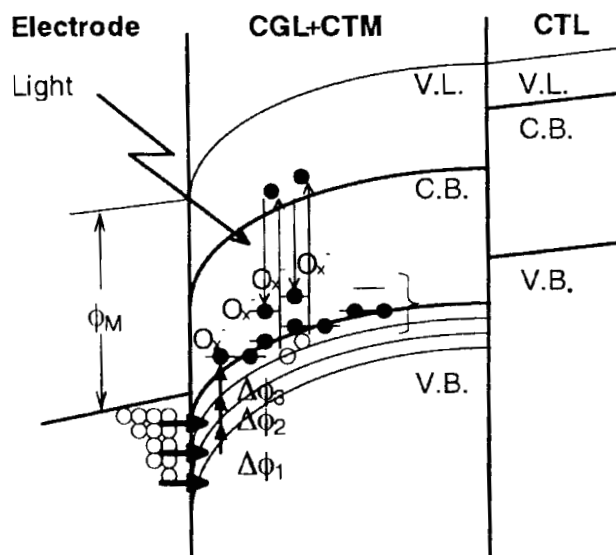
Figure 17(c). Hole injection from electrode to photoconductive layer during light exposure with applied voltage. ○hole, ● electron

cally appears when a CGM with a large ϕ_{CGM} is mixed with a CTM with a small ϕ_{CTM}, which suggests that charge transfer complexes form between the CGM and the CTM. However, this phenomenon requires further clarification.

Photocurrent Amplification Mechanism Based on Band Model

Figure 17 shows a schematic diagram explaining the effect that the CTM and oxygen have on hole injection at the electrode/photoconductive layer interface and on photocurrent amplification.

Figure 17(a) shows the state of an Elgraphic photosensor after being stored for several days in air

after fabrication. A CTM (DBB) with a small ϕ_{CTM} is mixed into the CGL, and the high carrier generation efficiency makes it possible for a large number of space charges to exist at room temperature. The photoconductive layer has a 1.08 eV trap, which is assigned to oxygen absorption, and a deep 1.76 eV trap.

During storage in air, CTM molecules with a small ϕ_{CTM} are ionized to form electron traps. Some of the electrons released in this process contribute to lowering the barrier to hole injection ($\Delta\phi_1$) by combining with oxygen to make an O_x^- absorbing layer at the electrode/photoconductive layer interface. Other electrons are trapped in the deep 1.76 eV traps and produce the space charge distribution. At the same time, thermally excited elec-

trons in the valence band are also trapped in the deep traps. These electrons probably raise the energy level of the valence band, and further lower the barrier to hole injection ($\Delta\phi_2$).

Figure 17(b) shows what happens when a positive voltage is applied to the ITO electrode, and a negative voltage to the Au electrode on the opposite side. Under these conditions, holes generated in the photoconductive layer migrate to the opposite electrode; and holes are injected from the ITO electrode and migrate toward the opposite electrode. Some of the trapped electrons recombine with holes and disappear; but other electrons remain trapped in the photoconductive layer.

Figure 17(c) shows what happens when the photosensor is exposed to light under the conditions just described. Photocarriers are generated in illuminated regions, and holes produced there migrate toward the opposite electrode. But released electrons are captured in deep 1.76 eV traps. This further lowers the injection barrier ($\Delta\phi_3$), thereby increasing the injection of holes from the ITO electrode. The photoinduced current (dark current subtracted from photocurrent) thus exceeds the photocurrent produced by illumination, and the apparent quantum yields exceeds unity, providing the photosensor with a large gain.

Conclusion

Photocurrent amplification, which means that the quantum yield exceeds unity, was observed in the organic photosensor used in Elgraphy, a novel image acquiring system. The quantum yield rises and exceeds unity within 30 msec after illumination begins when a 10 V/μm bias is applied. Under continuous illumination, the quantum yield exceeds one even when the voltage is as low as 3 V/μm.

In the photocurrent amplification capability, it has been demonstrated that the work function of the electrode material (ϕ_M) and ionization potential of CTM (ϕ_{CTM}) are closely related to the electrical characteristics of the photosensor. Photocurrent amplification was observed when the work function of the electrode was greater than 4.60 eV and the ionization potential of the CTM was greater than 5.40 eV. This process has been shown to involve atmospheric oxygen and acceptors.

TSC measurements of a CGL on which layers of a CTM with a small ionization potential were stacked revealed the existence of multiple electron trap levels deeper than 1 eV. The authors propose that the thermally generated and/or photogenerated carriers trapped in these electron traps lower the hole injection barrier at the electrode/photosensor interface, thus causing both a gradual increase in the dark current over time and also photocurrent amplification. ▲

References

1. M. Utsumi, M. Akada and E. Inoue, in *IS&T's 48th Annual Conference*, IS&T, Springfield VA, 1995, p. 499.
2. M. Akada, D. Aoki, H. Kamiyama, and E. Inoue, in *IS&T's 49th Annual Conference*, IS&T, Springfield VA, 1996, p. 290.
3. H. Kamiyama, M. Utsumi, H. Hikosaka, M. Akada, T. Toida, M. Mastuo, and E. Inoue, *J. Imaging Sci. Technol.* **44,** 45 (2000).
4. D. Aoki, S. Sakano, M. Okabe, O. Shimizu, M. Utsumi, M. Akada, and E. Inoue, in *IS&T's 48th Annual Conference*, IS&T, Springfield VA, 1995, p. 502.
5. K. Nakatani, J. Hanna and H. Kokado, *Electrophotography* **24**, 2 (1985).
6. K. Nakatani, J. Hanna and H. Kokado, *Electrophotography* **24**, 8 (1985).
7. E. Miyamoto, Y. Yamaguchi and M. Yokoyama, *Society of Electrophotography*. **28**,364 (1989).
8. M. Hiramoto, T. Miyao and M. Yokoyama, *Appl. Phys. Lett.* **57**, 625 (1990).
9. J. Mizuguchi, *Jpn. J. Appl. Phys.* **20**, 713 (1981).
10. A. H. Booth, *Can. J. Chem.* **32**, 214 (1954).